Influences of matrix strength and weak planes on fracture response of recycled aggregate concrete

Sourav Chakraborty , Kolluru V. L. Subramaniam [*]

Department of Civil Engineering, Indian Institute of Technology Hyderabad, Hyderabad, TS 502285, INDIA

ABSTRACT

The fracture behaviours of concrete made with natural aggregate and recycled coarse aggregate (RCA) derived from crushing old concrete are compared. The performances are evaluated using concrete proportioned for different compressive strengths. The RCA from crushed old concrete produces a composite aggregate with mortar and aggregate phases. An examination of the RCA shows pre-existing cracks in the aggregate phase. Crack propagation and crack opening profiles in the fracture response of concrete beams are evaluated using the Digital Image Correlation (DIC) technique. The displacement profiles across the beam obtained using DIC are evaluated to understand the crack growth in the concrete. The cohesive stress response and an energy measure determined from the fracture test are related to physical observations of the fracture surface. The crack path in the concrete and the contribution of the different interfaces depend on the strength of the matrix surrounding the aggregate. In concrete with lower cementitious and higher water contents, the new mortar interface with RCA and the pre-existing cracks in the RCA contribute to the fracture surface in the RCA. While a larger fracture surface area is created in concrete made with RCA, the energy measure and the cohesive stress determined from the fracture test are lower. In concrete proportioned for higher compressive strength, there is a densification of the RCA-mortar interface and the fracture plane is produced through the aggregates. The pre-existing cracks in the RCA create weak planes, which contribute to the fracture surface created. Improving the mortar-RCA interface does not result in an improvement in tensile strength or fracture characteristics since there is also a significant contribution of the weak planes in the aggregate phase of RCA to the failure surface. The measured fracture surface area does not correlate with the energy measure from fracture test response.

1. Introduction

Recycled Coarse Aggregate (RCA) retrieved from demolished concrete structures are increasingly being used to replace virgin natural aggregate. The use of RCA in concrete is required to meet the demand for producing concrete with diminishing supplies of natural stone and to reduce the environmental impact of producing natural aggregate from the environmental and economical points of view. Additionally, concrete made with RCA provides a solution for the beneficial utilisation of construction debris and helps reduce the environmental impact associated with the process of extracting natural coarse aggregate. Design codes permit the use of RCA in structural concrete . For instance, the Indian Code of practise [18] permits up to 20 percent replacement of natural aggregate with RCA.

The primary sources of recycled aggregate are demolished buildings, broken pavements, and tested concrete from laboratories

[3–6,8,20,24,33]. Production of RCA from demolished concrete typically involves separating other materials such as wood, steel, and brick from the debris. The production process of RCA involves further crushing and grading. After analysing the market opportunity and recycling options, portions with similar ingredients are broken together to reduce the separation process [39]. Reducing an existing concrete structure into larger pieces of concrete and further crushing results in fracturing the composite material into aggregate-sized pieces. The production process results in pieces of concrete containing portions of old aggregate with adhered mortar through a complex fracturing process. Therefore, the RCA is piece of the original composite material and is made up of multiple phases identified with aggregate and mortar in the original concrete. The surface of the RCA is made up of fracture planes through the aggregate and mortar in the original concrete.

Interfaces play a crucial role in determining the properties of concrete made with RCA, recycled aggregate concrete (RAC). RAC has

---

interfaces between the three distinct phases: the parent aggregate, the old residual mortar, and the new mortar [7]. Due to the adhered mortar portion, RCA is typically more porous, resulting in greater water absorption. Large amounts of water are absorbed by the pores in adhered mortar, reducing the workability and contributing to the low strength of concrete [20,37] . The water absorption and the rough texture of the RCA, however, contribute to a greater increase in compressive strength in the early ages [10].

Typical assessment of concrete is based on compressive strength. When an RCA is placed in a mortar of low strength, a weak interface is formed between the old and new mortars. A highly porous interfacial transition zone (ITZ) forms at the old and new mortar which fails at low stress. For RAC with compressive strength between 25 and 40 MPa, the ITZs formed with new mortar are the weak links, which contribute to a reduction in strength compared to natural aggregate. For concrete with a compressive strength greater than 40 MPa, there is significant aggregate fracture. Methods for enhancing the compressive strength of RCA have focused on enhancing the interface between the RCA and new mortar [21,25,29,32,30–31,37,41,45,46]. Improvements in compressive strength with interface modification, however, result in a smaller increase in the tensile strength. The split tensile strength is less sensitive to replacement levels than the compressive strength [10,41].

With change in matrix strength, the packing near the ITZ also changes, which has an effect on fracture behaviour of the concrete. The fracture energy of RAC is reduced by up to 40 percent compared to NAC, which has been attributed to the increase in porosity with RCA [22,24]. With higher matrix strength of concrete, more of the coarse aggregates break, changing the failure mechanism. The change in the crack path has an influence on the ductility and the fracture parameters of the concrete. Although there are studies available on the effect of matrix strength on the compressive strength of the RAC, the influence of matrix strength on the fracture mechanism in RCA is not understood. The effect of crack propagation through the various interfaces on the observed changes in the cohesive fracture response of RAC remains to be determined for different matrix strengths.

Crack propagation during tensile fracture of RAC of different compressive strengths is evaluated. The effect of RCA on fracture behaviour of concrete is studied for two different grades of concrete. The cracking in concrete is evaluated for the influences of the matrix strength, the ITZs and internal cracks present in the coarse aggregate. In normal strength concrete made with natural aggregate, the fracture-crack goes through the weak ITZ planes, while in case of high strength concrete, due to the improved matrix and denser packing of the fines, the aggregate start breaking, changing the crack propagation mechanism. To understand the effect of RCA replacement on the fracture mechanism more holistically, it is necessary to study the dual effect of matrix strength and RCA replacement. The specific objectives of this work are to determine the influence of RCA on fracture response, cohesive stress-crack opening relationship, crack extension-crack opening relationship, and fractured surface area. Specifically, the influence of RCA on crack growth is evaluated for normal and high-strength concrete. The impact of the interfaces in the concrete on crack growth and fracture behaviour are assessed. The impact of RCA on the fractured surface and the mechanism of failure is also evaluated.

2. Experimental program

Concrete was made using coarse aggregate in two size fractions of 10 and 20 mm. Both natural aggregate derived from crushed stone and RCA aggregate were used in concrete mixtures. Concrete mixtures were proportioned for achieving target mean strengths of 38 and 58 MPa using natural aggregate. The natural aggregate was crushed gravel. The specific gravities of the 10-mm and 20-mm size fractions were 2.64 and 2.66, respectively. The water absorption was 0.3 % and 0.5 %, respectively, for the 10 and 20-mm size fractions of the natural aggregate. The 10 and 20-mm natural aggregate had an impact resistance determined as

per Standard (*IS.2386 (Part IV)-1963* [28]) of 11.26 % and 5.56 %, respectively.

The RCA used in this study came from the demolition of a concrete building. A pneumatic jackhammer was used to break up the concrete structure into large pieces. Crushing of the big concrete block, magnetic separation, and vibration screening were the main steps in producing the recycled aggregate. After the building was taken down, the concrete blocks were broken up and crushed with a jaw crusher. The iron scraps were then taken out with a magnetic separator. Fine and coarse aggregates were separated using a vibrating screen [1]. The water absorption of the 10-mm size fraction was 6.88 %, while it was 2.04 % for the 20-mm size fraction. The 10-mm and 20-mm pieces of RCA had specific gravities of 2.34 and 2.47, respectively. The impact resistance measured from the 10-mm and 20-mm size fractions of the RCA was 25.73 % and 13.73 %, respectively. The RCA satisfied the requirement for use as aggregate in concrete (IS 383–2016) with an resistance less than 30 %.

The RCA was predominantly made up of broken concrete with some broken bricks. Each aggregate consisted of parent aggregate and adhering mortar from the old concrete. The RCA had cleaved fracture surfaces showing breakage of the parent aggregate. The leftover mortar adhering to the aggregate in the RCA varied in the aggregate. The leftover mortar in the aggregate was 12.45 % for the 10 mm size fraction and 11.79 % for the 20 mm size fractions [10]. More mortar was left on aggregates in the size range of 4.75 mm to 10 mm than on aggregates in the 10 to 20 mm size range. The smaller aggregates have a larger surface area per unit volume with a larger adhered mortar fraction than larger aggregates.

Table 1 shows the mass proportions of the mix for the concrete made with normal aggregate. The aggregate masses are shown in the saturated surface dry (SSD) condition. Concrete made with natural aggregate is referred to as Natural Aggregate Concrete (NAC). The compressive strength of concrete made with NCA is referred to as the grade of concrete. The procedure in IS 10262 - 2019 [27] (was used to proportion the concrete for a given strength. The concrete mixtures were proportioned for characteristic compressive strengths of 30 and 50 MPa and are referred to as M30 and M50 grades of concrete. The M30 and M50 grades of concrete made with NAC are referred to as M30-NAC and M50-NAC, respectively. The mean 28-day compressive strength of the M30-NAC and M50-NAC obtained from 150 mm cubes were 42.8 and 58.95 MPa, respectively. The aggregate contents and the composition of the cementitious binder were changed to achieve the desired compressive strengths from the NAC. Higher strengthwas achieved with a higher cementitious content and a lower water content, which increases the strength of the mortar matrix surrounding the coarse aggregate. The increase in the fines also results in better densification of the matrix.

Concrete mixtures were also made with RCA following the same proportions as for normal aggregate. The NAC was replaced with RAC while maintaining the same mortar composition in a concrete mixture of a specific grade. The concrete mixtures prepared with RCA are labelled as M30-RAC and M50-RAC. The RCA concrete mixtures contain RAC in a mortar matrix proportioned for target mean strengths of 30 and 50 MPa. The average 28-day compressive strengths recorded from 150 mm cubes of the M30, and M50-RAC were 36.6 and 42.52 MPa, respectively.

The concrete was prepared in a drum mixer. The dry ingredients were mixed for 2 min before adding water. The aggregates were used in

Table 1
Mass proportions by mass for 1.0 m^3 of the concrete mixture.

Grade of Concrete	Fine Aggregate	20 mm Coarse Aggregate	10 mm Coarse Aggregate	Fly ash/ Slag	Cement	Water
M30	836	610	499	108 (Fly ash)	252	180
M50	706	488	488	165 (Slag)	385	176

their oven-dry state, and the extra water needed for absorption to reach the SSD condition was added. The concrete was used to prepare standard 150 mm cubes and beams of 150 mm cross-section and 500 mm length.

2.1. Fracture test

Fracture testing was performed on notched beams which were tested in flexure under centre-point loading. The testing was performed using a servo-hydraulic closed-loop test machine, according to EN 14651:2005. Prismatic beams of 150 mm cross-section and 500 mm length were used. A 25 mm notch that was 2 mm wide was cut using a circular wet saw. The beams were tested over a span of 450 mm. Fig. 1 shows the test set-up. The testing was conducted in CMOD control at a prescribed rate of 0.05 mm/min. During the test, a Linear Variable Differential Transformer (LVDT) was attached to a fixed frame outside the beam to measure the center-point deflection.

The digital image correlation (DIC) technique was used to get the full-field surface displacement. DIC works by comparing the image of the object before it was deformed and the image of the object after it was deformed. Before the fracture test , a sprayed-on speckle pattern was prepared on the surface of the specimen. The beam was painted white and a mist of black paint was sprayed to make a random pattern of spots.

A 5-megapixel camera with a 50 mm lens was used to take digital pictures of the specimen for use in DIC. The camera was placed at a distance of 1 m from the sample and was facing the surface of the sample straight on. The physical calibration of the images was performed, and it was established at 13 pixels per millimetre for the imaged area of the specimen. For the test setup, the random error in the measurement was determined to be in the range of 0.02 pixels. Before the test began, a "reference image" was taken of the beam in the undeformed state prior to the application of load. During the fracture test, digital images of the specimen were taken at regular intervals and saved so that they could be looked at later.

Cross-correlation analysis was performed on the digital images of the beam specimen captured at different points in the fracture test response. Spatial domain cross-correlation was performed in VIC 2D^{TM} software to obtain full-field surface displacements. The displacement was determined from the correlation performed using subsets of 35×35 pixels [17], [44], [43]. A quantic B-spline interpolation of the grayscale values was used to get accuracy down to the sub-pixel level. The strain field was
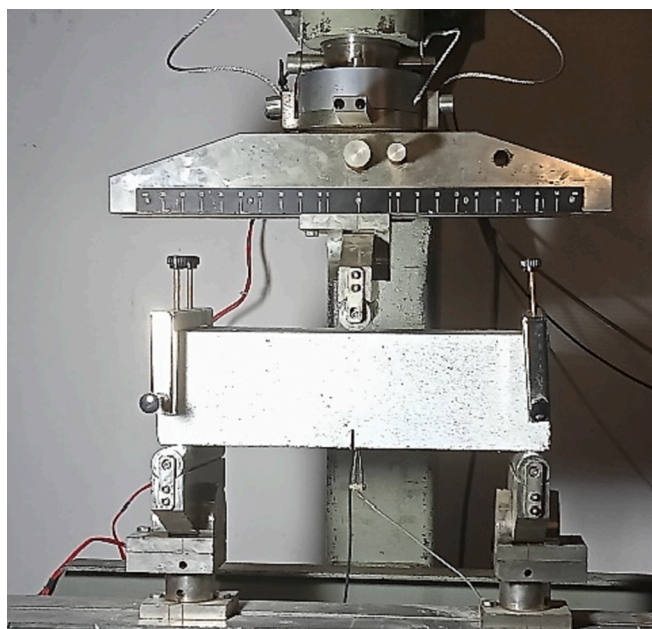
calculated as the gradient of the measured displacement field. With the test setup, 1.54 μm and 7 με were the most conservative estimates for resolutions in the measured displacement and strain [11,42].

2.2. Fracture surface area measurement

The surface area created by the crack was measured from the fractured surface of the beam. A laser-based sensor was used to determine the profile of the fractured surface. For the measurements, a class-2 Helium-Neon laser was used. Optical triangulation is the procedure for this measurement of the optical microscope. A receiver optic, which is placed at a certain angle to the optical axis of the laser beam, shows the diffuse part of this point of light's reflection on a position-resolving element (CMOS) based on distance from the measuring object, fractured surface in this case. With an accuracy of 2 μm, the laser setup can measure distances between 50 mm and 150 mm. The sample was put on a moving platform that could be programmed and was moved by stepper motors. The information was collected on a grid that was 0.1 mm by 0.1 mm. The surface was scanned at a rate of 60 mm/min. Fig. 2 shows the set-up and a typical area that is scanned. Using the ILD 1320–100 Tool software, the data was collected at 0.01 s intervals. Scans were performed on two 50 mm × 50 mm overlapping areas from each beam.

3. Experimental results and analysis

Fracture responses of the concrete mixtures proportioned for different compressive strengths with NAC, the M30 and M50-NAC and the corresponding concrete mixtures made with RAC, M30 and M50-RAC are shown in Fig. 3. Responses shown are obtained as an average of four specimens and the ranges are shown with scatter-bars. In both M30 and M50 grades of concrete, there are noticeable differences in the fracture responses from RAC compared to NAC. There is clearly a difference in the pre-peak response and the peak loads from the RAC are lower than the corresponding NAC. There is a significant reduction in the overall energy indicated by the area under the fracture load response on replacing NAC with RAC.

3.1. Cohesive stress response

The cohesive stress-crack separation (σ -w) relationships were derived from measured fracture test responses using a previously developed inverse analysis approach [16][15]. The inverse analytical approach has been utilised to extract the cohesive stress response of steel fibre-reinforced concrete [23] and, more recently, the early-age response in fibre-reinforced concrete [9]. In the inverse analysis, the cracked-hinge idealisation is utilised to forecast the load–deflection response of the beam [38]. In the cracked hinge representation, a cracked beam is represented as an elastic beam with a limited length hinge. The length of the hinge was determined to be 40 mm based on measurements [15]. The nonlinearity produced by the cohesive crack is represented using springs with defined σ-w relation. Crack opening displacement contributes to the total deformation of the hinge, and deformation compatibility is enforced between the elastic beams and the hinge. The equilibrium response of the beam is determined by gradually extending the cohesive crack within the hinge. The references [9]; [15]; [23] provide a detailed explanation and development of the prediction of the load-CMOD response of a beam evaluated in a three-point load configuration with a multilinear representation of the (σ-w) relationship. The cohesive σ-w response is represented as piecewise linear at discrete crack separation values in the multilinear representation. The number of (σ-w) segments can be altered to produce a smooth representation of the underlying cohesive relationship.

The load-CMOD response is extremely sensitive to the tensile strength (f_t) and the initial slope of the stress-crack relationship [15]. Typical σ-w relationships for concrete demonstrate a steep decline within a narrow range of w around f_t. Following the first quick fall σ,
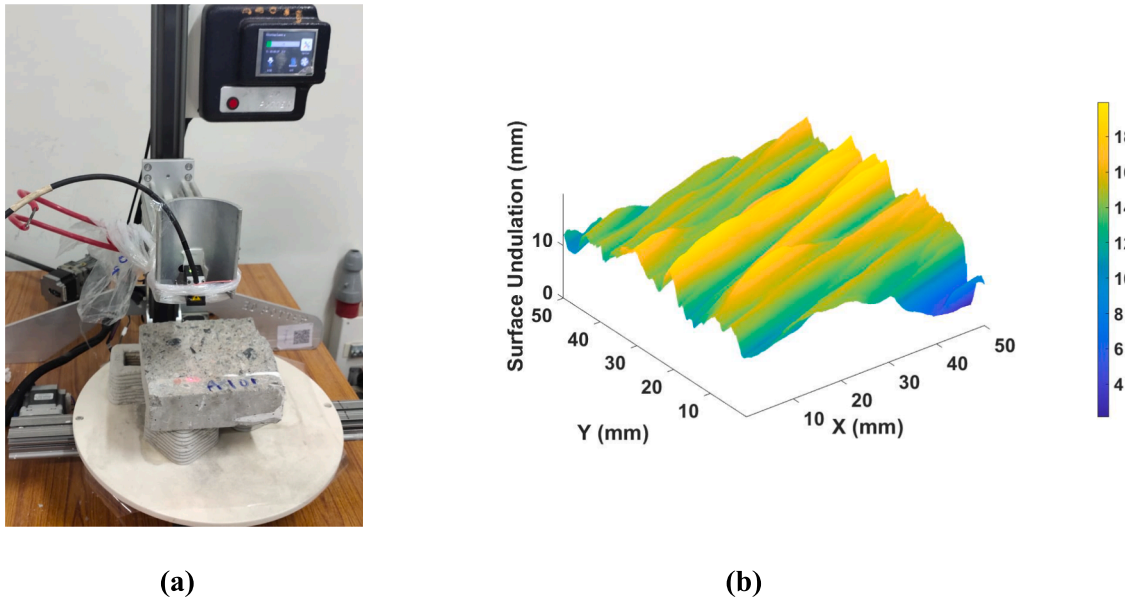

Fig. 1. Experimental setup for Fracture testing.

Fig. 2. (a) Experimental setup for laser displacement sensor **(b)** Typical scanned area.
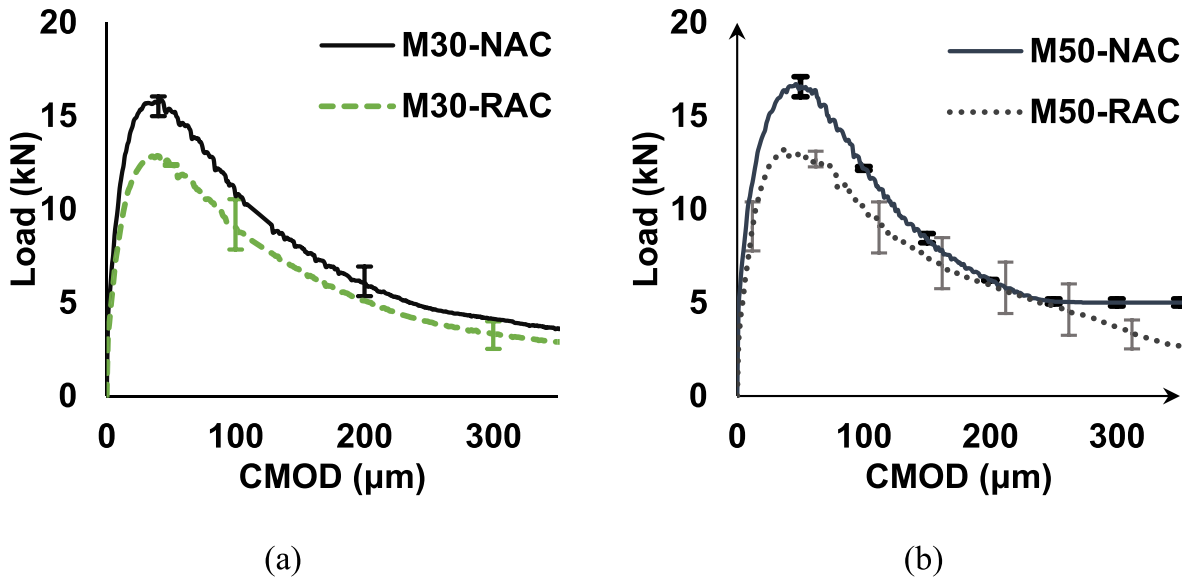

Fig. 3. Fracture response of NAC and RAC for **(a)** M30; and **(b)** M50 grade of concrete.

there is a long tail that extends across a wide range. In the tail section, σ decreases gradually as w increases.

To estimate σ as a function of w with the appropriate sensitivity, a three-step analysis was performed. In the first stage, the load-CMOD response up to 0.008 mm CMOD was used. The σ -w curve was determined up to a CMOD of 0.1 mm in the second stage. In the second stage 0.008 mm to 0.1 mm were considered. In the third stage, the remaining portion of the load response was used to determine the σ-w relationship. The goal function was a least-squares residual between the measured and forecasted load responses. There were two distinct objective functions employed. In the first and third stages, the goal function employed was

$$Norm = \frac{1}{n}\sqrt{\sum_{i=1}^{n}\left(P_i^{experimental} - P_i^{theoretical}\right)^2} \qquad (1)$$

where $P_u^{experimental}$ represents the experimentally determined peak load

and $P_u^{theoretical}$ represents the mathematically determined peak load. $P_i^{experimental}$ and $P_i^{theoretical}$ are the ith loads at the specified CMOD values in the experimental and predicted load responses, and n is the number of CMOD load points from 0.008 mm to 0.1 mm.

In the third stage, the other cohesive stress values at predetermined crack openings for displacements up to a CMOD of 0.3 mm were calculated. For generating the second stage of the σ-w response near the peak using the load response up to a CMOD of 0.1 mm, the goal function employed was

$$Norm = \left|\left(P_u^{experimental} - P_u^{theoretical}\right)\right| + \frac{1}{n}\sqrt{\sum_{i=1}^{n}\left(P_i^{experimental} - P_i^{theoretical}\right)^2} \qquad (2)$$

The corresponding predetermined σ at the chosen values of w were obtained by optimising with constrained minimisation and the interior point procedure. The initial stage consisted of determining the value of f_t and the ordinate of the initial softening response b_2 up to a CMOD value

of 0.05 mm. In the second step, σ was determined for w values of 0.10, 0.15, 0.25, 0.25, and 0.3 mm. One example of experimental and predicted load-CMOD responses with its corresponding cohesive stress-crack opening relationship is shown in Fig. 4.

Fig. 5 shows the σ-w relationship obtained from the inverse analysis by matching the experimental and predicted fracture responses. The residual stress as a function of crack opening from the cohesive relationship for each specimen has been normalised with the respective tensile strength (f_t). The intercept of the cohesive relationship is therefore set to one. The range in the cohesive stress obtained from the different specimens is shown by scatter bars around the average. The cohesive response indicates a very rapid decrease in the residual stress with crack separation. The σ decreases to a value close to $0.2f_t$ by the crack opening of 0.1 mm. Specific aspects of the cohesive behaviour indicate that the softening in the normal aggregate concrete is identical; a nominally similar response is obtained from both M50 and M30-NAC. The recycled aggregate concrete, initially, exhibits a more rapid decrease in the stress with crack opening compared to normal aggregate concrete.

The values of residual stress corresponding to their CMOD values and tensile strength are tabulated in Table 2. For a given mortar strength, the tensile strength (f_t) decreases with the use of RCA. The decrease in the tensile strength is, however, not as sensitive as the measured decrease in the compressive strength. The decrease in the tensile strength with the use of RCA is 13.4 and 9 % for the M30 and M50 grades of concrete, while the corresponding decreases in the compressive strengths were 14.48 and 25.33 %, respectively. In absolute values, the very rapid decrease in the cohesive stress up to 0.1 mm crack opening is evident.

Fig. 6 shows the fractured surface area measured from the notched beams tested in three-point flexure test. There is clearly a decrease in the fracture surface on increasing the grade of concrete. This is observed for concrete made with both NAC and RAC. The results follow expected trends, where an increase in the mortar strength results in a smoother fracture plane. Comparing the fracture surface areas of M30 grade concrete, there is however an increase in the surface area of M30-RAC compared to M30-NAC. For M50 grade of concrete, however, there is a small decrease in the fracture surface area with the use of RCA. The change in fracture surface due to change in matrix strength is more prominent compared to the effect of RCA replacement.
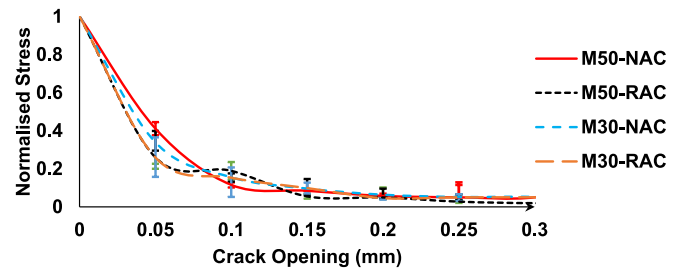

Fig. 5. Cohesive stress-crack opening relationship.

Table 2
Stress-crack opening relationships for M30 and M50 of NAC and RAC (Average values are listed with the variation shown in brackets).

| Crack opening (mm)	M30-NAC	M30-RAC	M50-NAC	M50-RAC
	Tensile strength, f_t (MPa)			
	3.71 (0.1)	3.21 (0.29)	3.89 (0.15)	3.54 (0.04)
	Normalised cohesive stress			
0.05	0.34 (0.06)	0.25 (0.10)	0.41 (0.03)	0.26 (0.06)
0.1	0.16 (0.02)	0.15 (0.10)	0.12 (0.01)	0.19 (0.04)
0.15	0.09 (0.05)	0.09 (0.03)	0.08 (0.01)	0.06 (0.01)
0.2	0.06 (0.03)	0.05 (0.01)	0.06 (0.01)	0.05 (0.05)
0.25	0.05 (0.01)	0.05 (0.02)	0.05 (0.08)	0.03 (0.01)
0.3	0.05 (0.07)	0.05 (0.05)	0.05 (0.1)	0.02 (0)
Normalised surface area	2.07 (0.08)	2.27 (0.07)	1.87 (0.07)	1.78 (0.02)
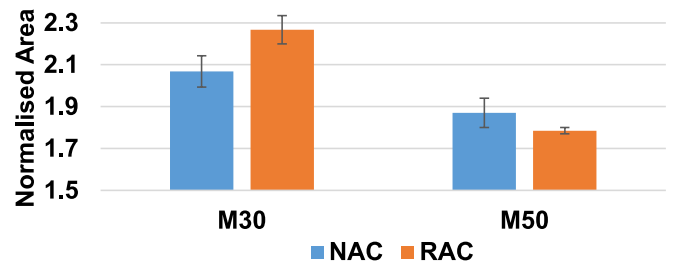
Fig. 6. Normalised fracture surface areas of NAC and RAC with different matrix strength.
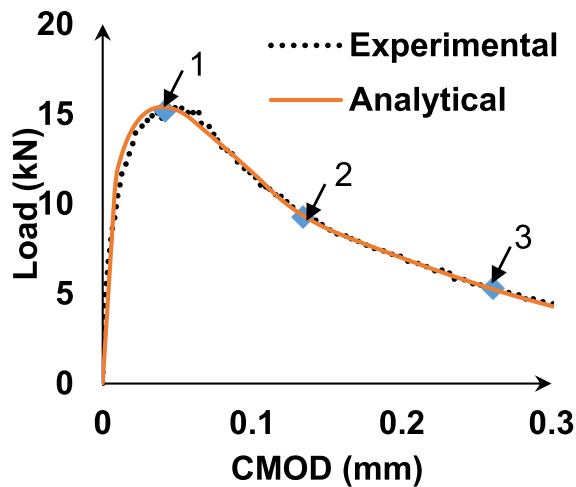
(a)
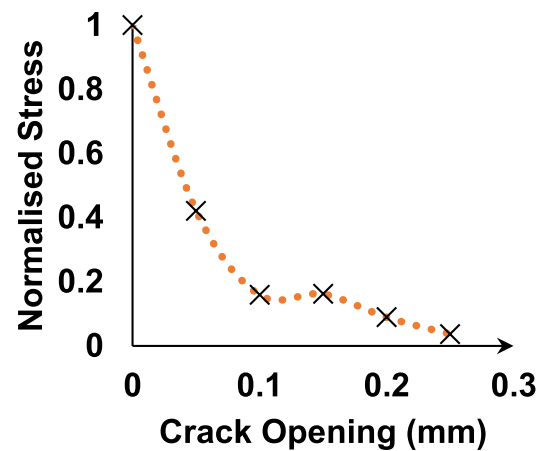
(b)

Fig. 4. (a) Comparison of experimental and numerically derived Load-CMOD response for M50 NAC; **(b)** Cohesive stress separation relationship of concrete as derived from Inverse analysis.

4. Analysis of crack growth

The crack growth in the fracture beams is analysed for comprehending the influence of the different aggregate on crack growth. The crack growth in the concrete of the different matrix strengths made with RAC and NAC was analysed using information from the digital image correlation. The crack depth and opening measured on the surface of the concrete beam were measured at different points in the load response. The process of determining the crack depth and opening is illustrated from the measured response of the beam shown in Fig. 4 (a). A coordinate system with its origin at the middle of the notch is utilised for analysis (as shown in Fig. 7 (a)). The X axis extends along the beam and the Y axis is along the depth. Fig. 7 shows the contours as well as the three-dimensional plots of displacement in the x-direction, U_x and longitudinal strain ε_{xx} at a load point 2 (Fig. 4 (a)) for a M50 NAC specimen. The crack is not directly visible to the naked eye. However, the discontinuity in the displacement contours directly above the notch shows physical separation produced by fracture. The displacement discontinuity is identified as a very sharp increase in displacement within a small region near the crack (values of X close to 0 mm) over a small distance. Away from the notch, U_x varies linearly with X. The displacement in the distant field is produced by bending. Within a small area near the crack, the ε_{xx} exhibit a very rapid localization with a sharp rise. The crack is identified with the rapid changes in the ε_{xx} within a small region.

The crack length and opening measurements are based on the detection of a physical discontinuity. Because of the fracture process zone, locating the crack tip is difficult due to the diffuse nature of the displacements within a small region close to the tip. An asymptotic matching procedure was developed to overcome this limitation [16]. The same procedure is followed here. The DIC analysis is performed using subsets of finite size. The size of the subset is chosen to provide accuracy in measurement while capturing the underlying gradients. The resolution of the DIC technique and the finite subset size limit the estimation of crack parameters from local displacements around a crack. In addition, there is a tiny loss of precision in a small region near the physical crack. Correlations are lost among the subsets that overlap with the physical opening produced by the crack. The correlations performed over overlapping subsets, resulted in a smearing of the physical boundary of the crack; this is seen in the form of a continuously varying displacement over the physical crack in Fig. 7 (a). To accurately measure the crack opening along a line with a given Y coordinate, the asymptote matching of far-field displacements was used [16]. The asymptotic far-field displacement along a line of constant Y coordinate is associated with flexure. As shown in Fig. 7 (a), the opening associated with the

physical separation caused by the break in the beam can be determined by the abrupt increase in U_x values along X. The displacement discontinuity along a line of constant Y coordinate was calculated from the difference between the far-field asymptotes on either side of the crack. Using the least-squares fit of a linear equation (linear equations with constant slope) to the far-field displacements on either side of the crack, the slopes of the lines were computed. The slopes of the two lines generated from linear fits to variations in far-field displacement with X coordinate do not differ significantly. The difference between the intercepts on the Y-axis of the two lines fitted to the far-field displacements was used to compute the displacement discontinuity induced by the crack.

The process of determining the displacement discontinuity is illustrated in Fig. 7 (a); the increment across a finite length centred at X = 0 is the displacement discontinuity. Crack opening displacements were estimated at various Y locations to establish the profile of the crack opening. The crack tip is found at the point on the profile of the crack opening where the displacement of the crack opening is zero. The process of identifying the crack opening profile along the depth of the beam is illustrated in Fig. 8 considering the responses at the load points identified in Fig. 4(a). It can be clearly seen that, along the length of the beam at X = 0 mm, there is a jump in the displacement profile. The displacement discontinuity marked as ΔU in the figure indicates the opening of the crack just above the notch at the given loading (at point 3 in the Fig. 4 (a)). The displacement discontinuity gets smaller along the depth of the beam.

The crack opening profile along the depth of the beam above the notch was generated from the measured crack openings with increasing Y. The crack displacement discontinuities and the corresponding crack profiles at three distinct points in the load response of the beam are shown in Fig. 8 (c). The measured crack discontinuity along the Y ordinate is the crack opening profile at the given load point. In the figure, the opening measured at the tip of notch corresponds with the crack tip opening displacement. The intercept of the measured opening displacement profile gives the location of the crack tip. It is observed that with increasing CMOD there is progressive upward propagation of the crack tip. Further, as the crack propagates along the depth of the beam, there is an increase in the crack opening displacement at any location along the depth. Since this is Mode I fracture, the crack path is nominally straight. There is no major deviation from a straight line extending above the notch. Small deviations from the straight path are due to the local heterogeneities.

Fig. 9 shows the changes in the mechanical work of fracture (W_F) and crack depth with increasing CMOD for the concretes of different compressive strengths made with NCA and RCA. The W_F was computed
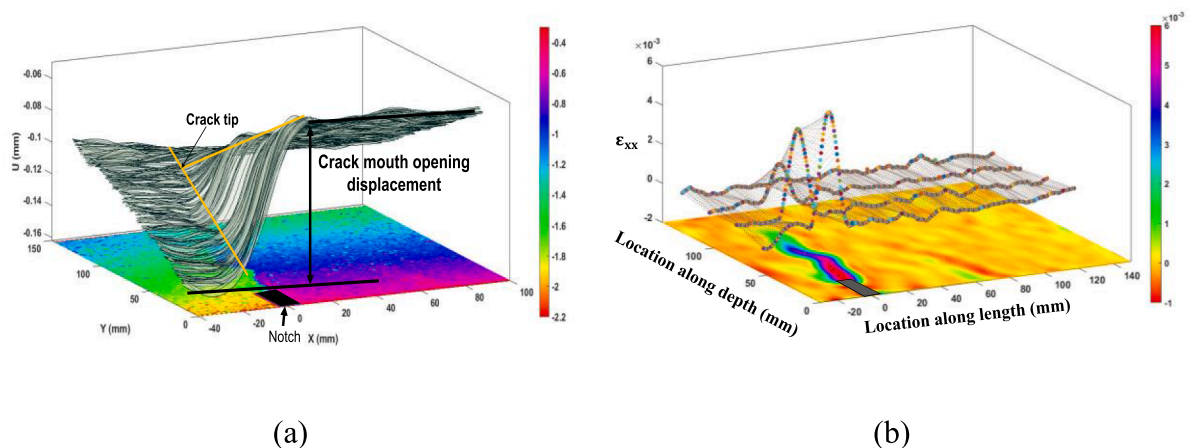

(a)

(b)

Fig.7. **(a)** Crack propagation and displacement contour from DIC with corresponding displacement profiles along the length of the beam. **(b)** DIC contour plot and variation in longitudinal strain near the crack region at different depths of the beam.
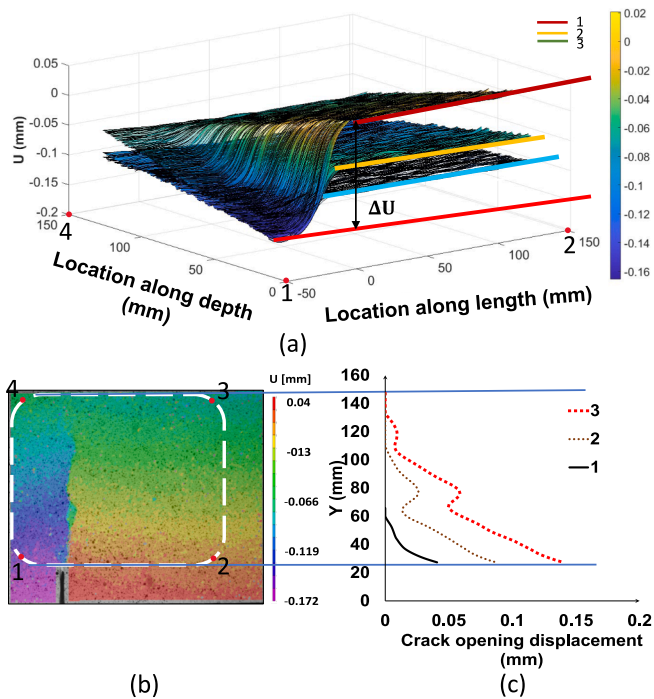
Fig. 8. (a) Variation of longitudinal displacement of the marked points near the crack region, (b) U_x from DIC image, and (c) Crack profiles at the marked points.

as the area under the fracture load response [13]. Consistently, there is a decrease in the W_F from NAC to RAC for both grades of concrete. The W_F of RAC is lower than NAC for all the values of CMOD. The difference in the W_F between the NAC and the RAC increases with the crack opening. The trends in the crack depth are, however, different. The measurement of crack depth indicates a consistently larger crack depth as a function of CMOD in M30-RAC compared to M30-NAC. While there is a significant scatter in the measurements, the difference between the crack depths measured with increasing CMOD remains essentially constant. The crack

depth measurements from M50 concrete indicates significant differences. Initially, at small CMOD, the crack depth in M50-NAC is significantly larger than the corresponding crack depth in M50-RAC. The difference decreases with increasing CMOD.

5. Discussion

The different phases present in the RAC were studied under a microscope and the existing state of the material and interfaces were evaluated. Fig. 10 depicts typical micrographs of M30-RAC and M50-RAC. The RAC was ground and polished to prepare the sample. Under an optical microscope, the different interfaces in the RAC can be clearly identified. The interface between the old mortar and the aggregate phase in the RCA is very dense. No separations or voids can be identified between the mortar adhering to the aggregate in the RCA. The RCA is produced by breaking and crushing old concrete, and the mortar is attached to aggregate by a strong interface, which is devoid of any weak planes. Several voids are, however, identified along the interface between the old and new mortar in the M30-RAC. A water-rich layer was likely formed at the interface between the old mortar in the RCA and the new mortar. The presence of voids along the interface indicates the formation of a water-rich layer, resulting in a weak interface. The new mortar interfaces in the M50-RAC are dense and do not exhibit any porosity or voids. The higher cementitious content in the M50 concrete results in higher densification of the interface. Several cracks are identified within the aggregate phase of the RCA. The aggregate portion of the RAC contains pre-existing cracks that were likely produced during the production process. The impact and the crushing operations produces RCA with surfaces which are identified with fractured aggregate and mortar phases in the existing concrete. The pre-existing cracks within the aggregate phase of the RCA are also the result of the production process.

Fig. 11 shows the fracture surfaces of M50-NAC and M50-RAC. The surface features and observations from corresponding areas in the broken counterparts were related to develop an understanding of the crack path during the fracture process. Red coloured shapes were marked to indicate the aggregates which were found broken after the test. Black shapes were used to mark the uncracked aggregates, which pulled out of the matrix. The natural aggregates used in the concrete
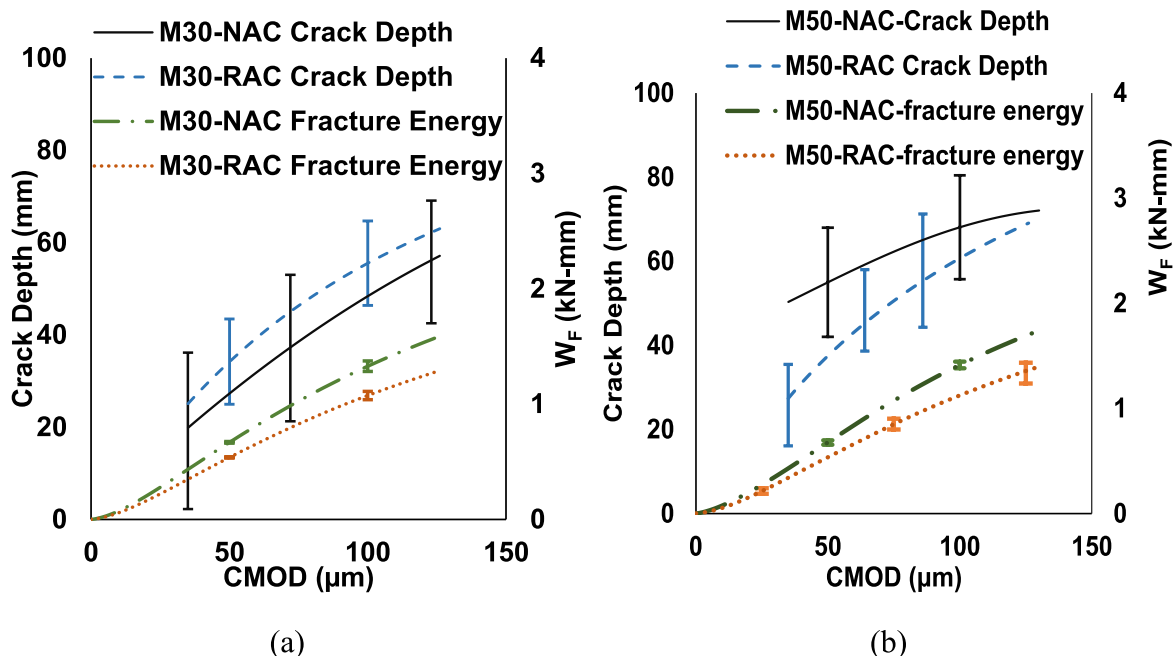

Fig. 9. **(a)** Variation of Fracture energy and crack depth between NAC and RAC with increasing CMOD for (a) M30, (b) M50 grade of concrete.
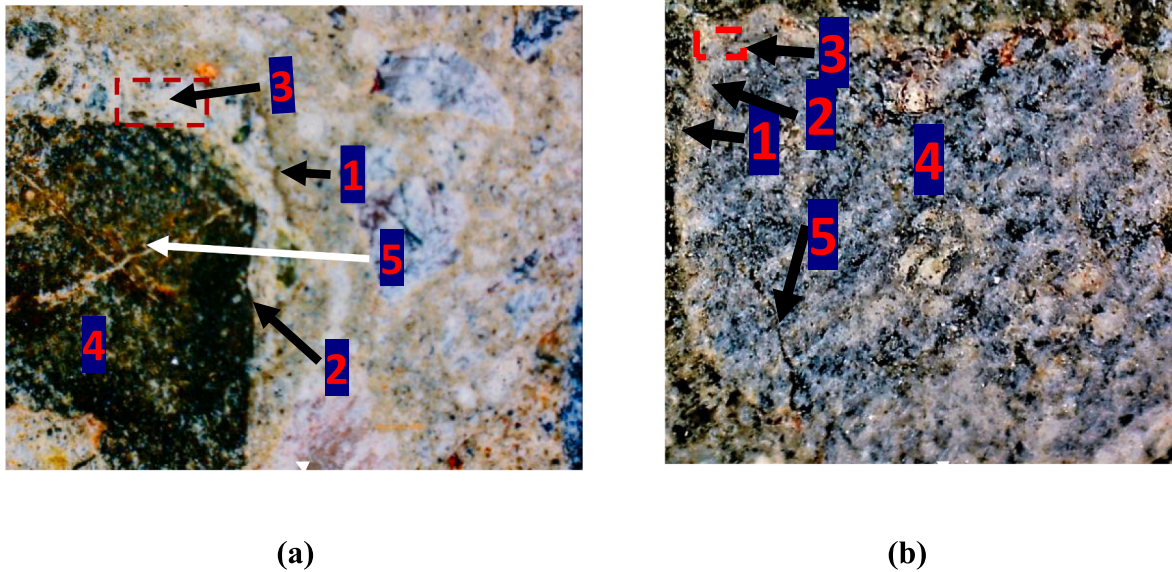
(a)   **(b)**

Fig. 10. Microstructure (a) M30 and (b) M50 showing different phases of RAC, 1 New ITZ; 2 Old ITZ; 3 Old Mortar; 4 Aggregate; 5 Existing cracked planes.

were strong enough that even for the M50 grade of concrete, a substantial number of aggregates remained unbroken. The fracture plane formed in the beams of M50-NAC consisted of surfaces created by the fractured agrgegate and the aggregate pullout. In M50-RAC, however, the fracture fracture plane was entirely made of fractured aggregate. This is clearly seen in the matching pieces of broken agrgegate in the two counterpart pieces of the broken beam.

The surfaces in the M30-NAC and RAC indicated clear difference in the mode of failure across the fracture plane on decreasing the strength of the matrix surrounding the coarse agrgegate. Observations from fracture surfaces in M30-NAC showed that most of the aggregate had pulled out. The crack had propagated through the interfaces between the aggregate and the mortar. The M30-RAC fracture surface, however, showed the presence of fractured aggregate in addition to the pullout of aggregate from the mortar matrix.

There are differences in the crack path and failure mechanisms observed in the fracture planes formed NAC and RAC. The fractured surface areas from both M50-NAC and M50-RAC are within the same range, though there is a small decrease in M50-RAC. In both cases, there is evidence of fractured aggregate in the fracture plane. The area created by the fracturing of aggregate is the same in both cases. However, not all the agrgegate were fractured in M50-NAC; A portion of the fracture plane passed through the aggregate-mortar interface. The total fracture surface in M50-NAC, therefore, consisted of fractured aggregate and the ITZ around the aggregate. The more tortuous path of the crack passing though the aggregate-mortar interface in M50-NAC contributes to the small increase in the fracture surface area compared to M50-RAC.

The higher fracture surface area in M30-RAC compared to M30-NAC can be explained considering the weak planes in the material. The crack propagation in M30-NAC creates a fracture plane that is predominantly through the interface between the NCA and the matrix. Fractured aggregate was not present in the fracture plane in M30-NAC. The weak planes in M30-NAC are therefore associated with the aggregate-mortar ITZ. In M30-RAC, the weak planes are associated with the interface between the old and new mortars. The fracture plane passes though the highly porous layer produced by accumulation of water at the interface between the mortars. In addition, the aggregates had internal cracking, which was introduced during the production process of the RCA. The weak planes along the crack path influence the crack path. The weak planes in the aggregate were aligned randomly with respect to the direction of crack propagation, resulting in an overall increase in the fracture surface area.

5.1. Correlating the different fracture measures and relating the observations from fracture specimens with fracture measures

Replacing NAC with RAC reduces the W_F of concrete proportioned for 30 and 50 MPa compressive strengths made with natural aggregate. There is also a more rapid decrease in the cohesive stress immediately following cracking with crack separation in M30-RAC/M50-NAC compared to M30-NAC/M50-NAC. The resistance to crack separation from the cohesive stress response is indicative of different failure mechanisms which contribute to the fracture plane. In the case of lower-grade concrete, the failure in the M30-NAC is along the interface between the aggregate and mortar. On replacing the NAC with RAC, the pre-existing cracks in the aggregate in M30-RAC contribute significantly to the overall fracture surface area created. The existence of the weak planes along the fracture plane contributes to the overall increase in the crack surface area in M30-RAC compared to M30-NAC. The weak planes in M30-RAC are of low toughness compared to the other interfaces in the material and do not contribute significantly to the fracture energy. In the concrete of a higher grade, M50-NAC, the failure is produced by aggregate fracture and pull-out from the matrix. This results in a smoother surface and a decrease in the fracture surface relative to M30-NAC. The weak planes of low fracture toughness associated with pre-existing cracks in the RCA contribute significantly to the fracture surface area while reducing the overall W_F.

The differences in the tensile strength and the cohesive stress are therefore controlled by the toughness of the weak planes in the material. The pre-existing cracks in the aggregate play a significant role in determining the fracture response of concrete in RCA. In lower-grade concrete the new mortar interfaces with old mortar and aggregate phases in RCA also constitute weak planes. In this work, the scale of observation relates to fracture observed using DIC, and this is linked with material at the *meso*-scopic level. The physical observations of weak planes associated with the ITZ and pre-existing cracks in the aggregate are shown to influence the overall fracture response. Bridging the length scales requires information about the toughness of the weak planes. This information can then be used in accurate mesoscopic models such as the phase-field approach for an accurate representation of the fracture processes. Different phase field models are available in this context to understand the effect of *meso*-scale changes, like introduction of internal cracks and different types of interfaces in the coarse aggregate in the overall fracture behaviour of the matrix [12,26,34,48], 2022). Recent studies using the phase field model have shown the
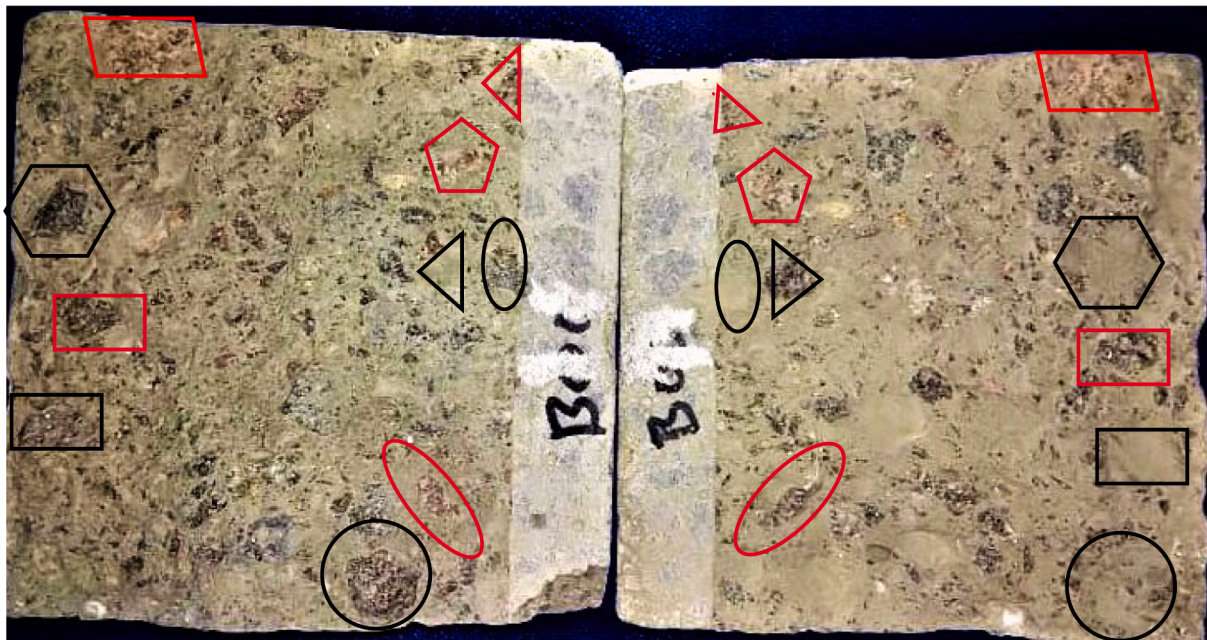
(a)

(b)

Fig. 11. Fractured surfaces of (a) NAC and (b) RAC of M50 grade concrete.

significant influence of interface toughness at a bi-material interface on determining the direction of crack propagation [19,40]. However, for implementing the phase field-based numerical models, the interface fracture toughness of the interfaces is a critical parameter. Also, such an implementation would require consideration of pre-existing cracks in the aggregate.

In the concrete proportioned for 30 MPa compressive strength with NCA, while a larger fracture surface area is created, there is an overall decrease in the W_F measured from M30-RAC as a function of the crack mouth opening. The W_F is plotted as a function of the crack length in Fig. 12. While there is significant scatter in the data, there is an increasing trend in the W_F for crack advance with increasing crack length. The values from both M30-RAC and M30-RAC are comparable. In the M50 grade concrete, a larger fracture surface area is created in M50-NAC, which also has a higher W_F with increasing crack mouth opening. The crack depth in M50-RAC is, however, smaller than in M50-

NAC for a given crack mouth opening. The differences in the W_F per unit crack advance between M50-NAC and M50-RAC are not significant considering the offsetting influences of energy and crack length. Comparing between the two grades, there is clearly a larger increase in the W_F per unit crack advance in M50 grade of concrete than in M30 grade of concrete. Increasing the grade of concrete, therefore produces a more rapid increase in W_F with increasing crack length.

The available information is in agreement with the results in the literature. The improvements in the compressive strength achieved using different surface treatments of the RCA do not produce a corresponding increase in the tensile strength. For mechanical treatment of the RCA almost no improvement is found in the split tensile strength for both low and high grade of concrete [41]. PVA impregnated concrete is also unable to improve the split tensile strength for M40 grade of concrete [31]. Whereas adding silica fume or polymer modified surface or CO_2 curing of the RCA concrete individually produced 5 % to 10 %
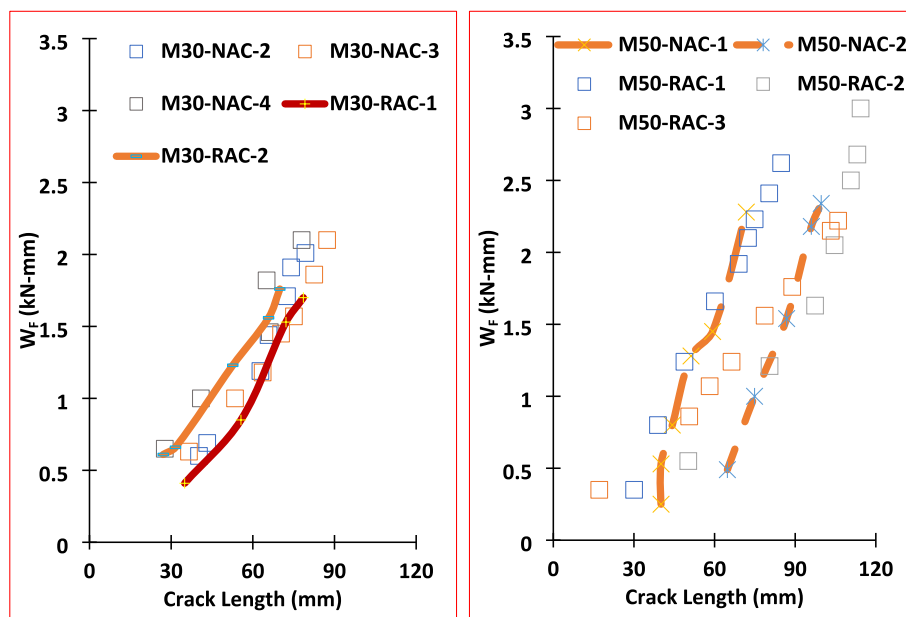
Fig. 12. Increase in W_F with crack length: **(a)** M30 grade concrete; **(b)** M50 grade concrete.

improvement each [21,32,45]. 0.1 M HCl solution treatment showed very good improvement in the compressive strength [29] but marginal improvement in the tensile strength [25,29]. In the present study also, improvement in the tensile strength due to better packing of fines near the RCA interface is 10.3 %. Surface treatment of the RCA and improvements in the interface between RCA and mortar do not contribute much to the improvement of the tensile strength of the concrete, because the pre-existing cracks in the RCA, which determine the failure in tension.

6. Conclusions

Fracture tests for NAC and RAC for M30 and M50 grades of concrete were conducted. Post cracking cohesive stress response was obtained using inverse analysis. The fracture surface area, crack depth, and fracture energy were evaluated as a function of crack propagation. The conclusions from the analysis and main findings are given below.

1. The RAC has a lower tensile strength than NAC for both grades of concrete. The decrease in the tensile strength is less sensitive to RCA replacement than the compressive strength.
2. The cohesive response indicates a more rapid decrease in the residual stress for RAC with the crack opening for the M30 grade and lesser stress loss in the M50 grade except for the initial loss.
3. The crack extension-crack opening indicates a larger crack depth in RAC than NAC for a similar crack mouth opening displacement in the M30 grade of concrete and a lesser crack depth for the same crack mouth opening displacement in M50 grade of concrete.
4. For crack penetration under the stress field produced by flexure, RAC requires less fracture energy with increasing crack mouth opening. However, in M30, a larger fracture surface area is created in RAC than in NAC due to a greater number of weaker planes and random alignment of those links compared to the vertical plane. The weak planes in the RAC are identified with the new mortar interfaces and pre-existing fracture planes in the aggregate. In M50 grade of concrete, new mortar to old mortar ITZ became stronger and pre-existing cracks in the RCAs became the guiding factor for the crack propagation creating an equal fractured surface area for both NAC and RAC.
5. In the M30 grade of concrete, RAC is more brittle than NAC, but with increasing matrix strength, RAC shows better performance in terms

of ductility and in the M50 grade of concrete, RAC becomes less brittle than NAC.

CRediT authorship contribution statement

Sourav Chakraborty: Investigation, Methodology, Writing – original draft. **Kolluru V. L. Subramaniam:** Conceptualization, Supervision, Writing – review & editing.

Declaration of Competing Interest

The authors declare that they have no known competing financial interests or personal relationships that could have appeared to influence the work reported in this paper.

Data availability

Data will be made available on request.

References

[1] Z. Abdollahnejad, M. Mastali, M. Falah, T. Luukkonen, M. Mazari, M. Illikainen, Construction and demolition waste as recycled aggregates in alkali-activated concretes, Materials 12 (23) (2019) 4016, https://doi.org/10.3390/ma12234016.
[3] M.P. Adams, T. Fu, A. Guerra, M. Morales, J.H. Ideker, O.B. Isgor, Cracking susceptibility of concrete made with coarse recycled concrete aggregates. 102 (2016) 802–810, https://doi.org/10.1016/j.conbuildmat.2015.11.022.
[4] S. Ahmad, W.M. Tech, B. Singh, Shear transfer strength of normal and high-strength recycled aggregate concrete – an experimental investigation, Constr. Build. Mater. 125 (2016) 29–40, https://doi.org/10.1016/j.conbuildmat.2016.08.022.
[5] M. Arezoumandi, A. Smith, J.S. Volz, K.H. Khayat, An experimental study on shear strength of reinforced concrete beams with 100 % recycled concrete aggregate, Constr. Build. Mater. 53 (2014) 612–620, https://doi.org/10.1016/j.conbuildmat.2013.12.019.
[6] M. Arezoumandi, A. Smith, J.S. Volz, K.H. Khayat, An experimental study on flexural strength of reinforced concrete beams with 100 % recycled concrete aggregate, Eng. Struct. 88 (2015) 154–162, https://doi.org/10.1016/j.engstruct.2015.01.043.
[7] M. Behera, S.K. Bhattacharyya, A.K. Minocha, R. Deoliya, S. Maiti, Recycled aggregate from C&D waste & its use in concrete – a breakthrough towards sustainability in construction sector: A review, Constr. Build. Mater. 68 (2014) 501–516, https://doi.org/10.1016/j.conbuildmat.2014.07.003.
[8] G. Belén, M. Fernando, M. Isabel, E. Javier, Structural shear behaviour of recycled concrete with silica fume, Constr. Build. Mater. 23 (11) (2009) 3406–3410, https://doi.org/10.1016/j.conbuildmat.2009.06.035.

[9] M.V. Bhogone, K.V.L. Subramaniam, Early-age tensile constitutive relationships for steel and polypropylene fiber reinforced concrete, Eng. Fract. Mech. 244 (2021), 107556, https://doi.org/10.1016/j.engfracmech.2021.107556.

[10] U.S. Biswal, P. Dinakar, A mix design procedure for fly ash and ground granulated blast furnace slag based treated recycled aggregate concrete, Cleaner Eng. Technol. 5 (2021), 100314, https://doi.org/10.1016/j.clet.2021.100314.

[11] H.A. Bruck, S.R. McNeill, M.A. Sutton, W.H. Peters, Digital image correlation using Newton-Raphson method of partial differential correction, Exp. Mech. 29 (3) (1989) 261–267, https://doi.org/10.1007/BF02321405.

[12] T.Q. Bui, X. Hu, A review of phase-field models, fundamentals and their applications to composite laminates, Eng. Fract. Mech. 248 (2021), 107705, https://doi.org/10.1016/j.engfracmech.2021.107705.

[13] N.B. Burud, J.M.C. Kishen, Response based damage assessment using acoustic emission energy for plain concrete, Constr. Build. Mater. 269 (2021), 121241, https://doi.org/10.1016/j.conbuildmat.2020.121241.

[15] K. Chiranjeevi Reddy, K.V.L. Subramaniam, Analysis for multi-linear stress-crack opening cohesive relationship: application to macro-synthetic fiber reinforced concrete, Eng. Fract. Mech. 169 (2017) 128–145, https://doi.org/10.1016/j.engfracmech.2016.11.015.

[16] K. Chiranjeevi Reddy, K.V.L. Subramaniam, Experimental investigation of crack propagation and post-cracking behaviour in macrosynthetic fibre reinforced concrete, Mag. Concr. Res. 69 (9) (2017) 467–478, https://doi.org/10.1680/jmacr.16.00396.

[17] T.C. Chu, W.F. Ranson, M.A. Sutton, Applications of digital-image-correlation techniques to experimental mechanics, Exp. Mech. 25 (3) (1985) 232–244, https://doi.org/10.1007/BF02325092.

[18] IS 383 -2106. Coarse and Fine Aggregate for Concrete—Specification, Bureau of Indian Standards, New Delhi, India, 2016.

[19] P. Dhaladhuli, R. Amirtham, J.N. Reddy, Interaction between interfacial damage and crack propagation in quasi-brittle materials, Mech. Adv. Mater. Struct. 29 (22) (2022) 3187–3208, https://doi.org/10.1080/15376494.2021.1891356.

[20] R. K, Dhir, J, de Brito, R. V, Silva, C. Q, Lye, Properties and Composition of Recycled Aggregates. In Sustainable Construction Materials 2019 (pp. 89–141). Elsevier. https://doi.org/10.1016/B978-0-08-100985-7.00005-4.

[21] H. Dilbas, M. Şimşek, Ö. Çakır, An investigation on mechanical and physical properties of recycled aggregate concrete (RAC) with and without silica fume, Constr. Build. Mater. 61 (2014) 50–59, https://doi.org/10.1016/j.conbuildmat.2014.02.057.

[22] H. Fallahnejad, M.R. Davoodi, I.M. Nikbin, The influence of aging on the fracture characteristics of recycled aggregate concrete through three methods, Struct. Concr. 22 (S1) (2021), https://doi.org/10.1002/suco.202000119.

[23] S. Gali, K.V.L. Subramaniam, Multi-linear stress-crack separation relationship for steel fiber reinforced concrete: Analytical framework and experimental evaluation, Theor. Appl. Fract. Mech. 93 (2018) 33–43, https://doi.org/10.1016/j.tafmec.2017.06.018.

[24] E. Ghorbel, G. Wardeh, Influence of recycled coarse aggregates incorporation on the fracture properties of concrete, Constr. Build. Mater. 154 (2017) 51–60, https://doi.org/10.1016/j.conbuildmat.2017.07.183.

[25] E. Güneyisi, M. Gesoğlu, Z. Algın, H. Yazıcı, Effect of surface treatment methods on the properties of self-compacting concrete with recycled aggregates, Constr. Build. Mater. 64 (2014) 172–183, https://doi.org/10.1016/j.conbuildmat.2014.04.090.

[26] X. Hu, H. Xu, X. Xi, P. Zhang, S. Yang, Meso-scale phase field modelling of reinforced concrete structures subjected to corrosion of multiple reinforcements, Constr. Build. Mater. 321 (2022), 126376, https://doi.org/10.1016/j.conbuildmat.2022.126376.

[27] IS 10262 -2019. Concrete Mix Proportioning - Guidelines, Bureau of Indian Standard, New Delhi, India, 2019.

[28] IS 2386 (Part IV) -1963. Method of Test for Aggregate for Concrete Part IV Mechanical Properties, Bureau of Indian Standard, New Delhi, India, 1963.

[29] H. Katkhuda, N. Shatarat, Improving the mechanical properties of recycled concrete aggregate using chopped basalt fibers and acid treatment, Constr. Build. Mater. 140 (2017) 328–335, https://doi.org/10.1016/j.conbuildmat.2017.02.128.

[30] S.-C. Kou, C.-S. Poon, Mechanical properties of 5-year-old concrete prepared with recycled aggregates obtained from three different sources, Mag. Concr. Res. 60 (1) (2008) 57–64, https://doi.org/10.1680/macr.2007.00052.

[31] S.-C. Kou, C.-S. Poon, Properties of concrete prepared with PVA-impregnated recycled concrete aggregates, Cem. Concr. Compos. 32 (8) (2010) 649–654, https://doi.org/10.1016/j.cemconcomp.2010.05.003.

[32] S.-C. Kou, B. Zhan, C.-S. Poon, Use of a CO2 curing step to improve the properties of concrete prepared with recycled aggregates, Cem. Concr. Compos. 45 (2014) 22–28, https://doi.org/10.1016/j.cemconcomp.2013.09.008.

[33] B. Marinkovic, N. Tošic, I.S. Ignjatovic, Shear behaviour of recycled aggregate concrete beams with and without shear reinforcement. 141 (2017) 386–401, https://doi.org/10.1016/j.engstruct.2017.03.026.

[34] L. Min, X. Hu, W. Yao, T.Q. Bui, P. Zhang, On realizing specific failure initiation criteria in the phase field model, Comput. Methods Appl. Mech. Eng. 394 (2022), 114881, https://doi.org/10.1016/j.cma.2022.114881.

[37] K. Musiket, M. Rosendahl, Y. Xi, Fracture of recycled aggregate concrete under high loading rates, J. Mater. Civ. Eng. 28 (6) (2016) 04016018, https://doi.org/10.1061/(ASCE)MT.1943-5533.0001513.

[38] J.F. Olesen, Fictitious crack propagation in fiber-reinforced concrete beams, J. Eng. Mech. 127 (3) (2001) 272–280, https://doi.org/10.1061/(ASCE)0733-9399(2001)127:3(272).

[39] S. Pantini, L. Rigamonti, Is selective demolition always a sustainable choice? Waste Manag. 103 (2020) 169–176, https://doi.org/10.1016/j.wasman.2019.12.033.

[40] D. Pranavi, A. Rajagopal, J.N. Reddy, Interaction of anisotropic crack phase field with interface cohesive zone model for fiber reinforced composites, Compos. Struct. 270 (2021), 114038, https://doi.org/10.1016/j.compstruct.2021.114038.

[41] P. Savva, S. Ioannou, K. Oikonomopoulou, D. Nicolaides, M.F. Petrou, A mechanical treatment method for recycled aggregates and its effect on recycled aggregate-based concrete, Materials 14 (9) (2021) 2186, https://doi.org/10.3390/ma14092186.

[42] H.W. Schreier, M.A. Sutton, Systematic errors in digital image correlation due to undermatched subset shape functions, Exp. Mech. 42 (3) (2002) 303–310, https://doi.org/10.1007/BF02410987.

[43] M.A. Sutton, S.R. McNeill, J. Jang, M. Babai, Effects of subpixel image restoration on digital correlation error estimates, Opt. Eng. 27 (10) (1988), https://doi.org/10.1117/12.7976778.

[44] M. Sutton, W. Wolters, W. Peters, W. Ranson, S. McNeill, Determination of displacements using an improved digital correlation method, Image Vis. Comput. 1 (3) (1983) 133–139, https://doi.org/10.1016/0262-8856(83)90064-1.

[45] P. Velardo, I.F. Sáez del Bosque, A. Matías, M.I. Sánchez de Rojas, C. Medina, Properties of concretes bearing mixed recycled aggregate with polymer-modified surfaces, J. Build. Eng. 38 (2021), 102211, https://doi.org/10.1016/j.jobe.2021.102211.

[46] J. Wu, Y. Zhang, P. Zhu, J. Feng, K. Hu, Mechanical properties and ITZ microstructure of recycled aggregate concrete using carbonated recycled coarse aggregate, J. Wuhan University of Technol.-Mater. Sci. Ed. 33 (3) (2018) 648–653, https://doi.org/10.1007/s11595-018-1873-1.

[48] P. Zhang, W. Yao, X. Hu, X. Zhuang, Phase field modelling of progressive failure in composites combined with cohesive element with an explicit scheme, Compos. Struct. 262 (2021), 113353, https://doi.org/10.1016/j.compstruct.2020.113353.